

Predicted and Measured Performance of the 62 m Span Norwegian Olympic Ice Hockey Cavern at Gjøvik

N. BARTON†
T. L. BY†
P. CHRYSANTHAKIS†
L. TUNBRIDGE†
J. KRISTIANSEN†
F. LØSET†
R. K. BHASIN†
H. WESTERDAHL†
G. VIK†

The feasibility of excavating caverns of very large span for underground siting of nuclear power stations in Norway was investigated in the early 1970s. In the end, the 1994 Winter Olympic Games provided the necessary impetus for utilizing a very large engineered rock cavern and proving its general feasibility. The 62 m span Olympic Ice Hockey Cavern was constructed in Gjøvik by Veidekke-Selmer JV in 1991. It is located in a jointed gneiss of average $RQD = 67\%$. The Q -values range from 1 to 30, with a weighted mean of about 9, i.e. fair quality rock. The cavern has a rock cover of only 25–50 m, thus posing challenging design problems. The investigations prior to construction included two types of rock stress measurements, cross-hole seismic tomography, geotechnical core logging, Q -system classification and numerical modelling with UDEC-BB. Predicted maximum deformations were 4–8 mm; these were surprisingly small due to the high horizontal stresses recorded. Extensometer (MPBX) installations from the surface prior to construction, precision surface levelling and MPBX installed from inside the cavern gave a combined measure of maximum deformations in the range 7–8 mm with the 62 m span fully excavated, and three adjacent caverns for the Postal Services also completed. Permanent rock reinforcement based on the Norwegian method of tunnelling (NMT), consisted of 10 cm wet process steel fibre reinforced shotcrete, and systematic bolting and cable bolting in alternating 2.5 and 5.0 m c/c patterns. Both the cables and bolting were untensioned and fully grouted.

INTRODUCTION

During the 1970s, NGI performed a series of siting studies and some *in situ* testing, to investigate the feasibility of underground siting of nuclear power plants. Special attention was focused on the need for a reactor containment cavern with a hemispherical domed arch of at least 50 m diameter. The Norwegian State Power Board (Statkraft) and subsequently also the Swedish

State Power Board (Vattenfall) and Sweden's BeFo organization funded parallel theoretical studies of large-span caverns at NGI.

Physical models of large spans in jointed rock were used to study the effect of medium and high horizontal stress levels and the effects of various joint orientations. Comparisons were also made with continuum FEM studies. Today, fifteen years later, we would probably have used discrete element methods such as UDEC, although the number of discrete blocks in the physical models (20,000) exceeds all but the most extreme discrete element models.

†Norwegian Geotechnical Institute (NGI), Oslo, Norway.

A brief review of some of the findings of these earlier studies will be used as an introduction to the real life problems subsequently encountered at Gjøvik, where a 62 m span cavern was successfully engineered for the 1994 Winter Olympic Games in Norway.

Prior to specific siting of large caverns, whether for nuclear reactor vessels or for Olympic ice hockey, estimates have to be made of stress levels and rock properties. Concerning stress levels, we elected to investigate low, medium and high stress as follows:

$$\frac{\sigma_h}{\sigma_v} = \frac{1}{3}$$

$$\frac{\sigma_h}{\sigma_v} = 1.0$$

$$\frac{100}{z} + 0.3 \leq \frac{\sigma_h}{\sigma_v} \leq \frac{1500}{z} + 0.5.$$

The latter (where z is the depth in metres) is based on measured data reviewed by Brown and Hoek [1]. The actual level chosen in the third case was $k = 20$ at 25 m depth and $k = 6$ at 100 m depth, i.e. a trapezoidal distribution of stress, within the above range of observations.

Figure 1 illustrates the FEM results obtained with an assumed rock cover of only 25 m, $E = 14$ GPa, $\nu = 0.1$ and plane stress conditions (equivalent to the two-dimensional physical models). For stage 2 of the excavation (roughly equivalent to the Olympic Ice Hockey Cavern dimensions) maximum vertical deformations for the three stress cases were 2.7, 1.5 and (–) 10.8 mm (i.e. heave). When the rock cover was increased to 50 m, the isotropic case ($k = 1.0$) showed a maximum downward deformation of 2.9 mm, i.e. the tendency for heave was, of course, reduced.

The physical models, which were described in detail by Barton and Hansteen [2], consisted of 20,000 blocks of discretely fractured model material, with two regular joint patterns of constant dip. These idealized, two-dimensional models were loaded by gravity and by vertical boundaries that resemble today's numerical roller boundaries. Figure 2 illustrates deformations measured in the central, near-cavern area of six physical models under hydrostatic (left) and tectonic (right) stress levels equivalent to two of the cases described above. The models with continuous horizontal and discontinuous vertical jointing showed only downward deformation of the arch, due to joint opening effects. It should be noted that the tension fracturing technique gave the two sets of joints (the first continuous, the second discontinuous) unusually high values of JRC (joint roughness coefficient). Stability without bolting was therefore ensured in the arch of the models, but not always in the walls. A model with a cavern excavated at twice the depth shown in Fig. 2 showed downward movement of the full-span top heading, followed by upward movement of the arch as wall height was increased.

The above numerical and physical models demonstrate the possible favourable nature of near-surface siting for large caverns, at least from the point of

view of possible high horizontal stress levels causing reduced deformation. A compromise would need to be arrived at in practice, involving near-surface siting but avoidance where possible of near-surface weathering and higher joint frequencies. (Cross-hole seismic tomography proved invaluable in this respect as will be seen later.)

FEASIBILITY OF AN OLYMPIC SPORTS HALL

The idea of locating an Olympic arena in rock was first conceived by Jan Rygh, the former Director of the Oslo consulting company, Fortifikasjon A/S, who, together with the City of Gjøvik, were responsible for project development and marketing during the 18 months from when the project was first presented until a contract agreement was reached. As is typical when one is extending the limits of experience and technology, the initial scepticism that had to be overcome was formidable.

The ice hockey cavern was to have a span of 60 m, a length of 90 m and a height of 25 m. The spectator capacity was to be 5400, making it by far the largest cavern for public use in the world.

In 1991, NGI and NOTEBY of Oslo, and SINTEF/NTH of Trondheim co-operated in the first phase of the geological and rock mechanics investigations with rock cavern designers Fortifikasjon A/S of Oslo as the client.

During this first phase of the feasibility studies, existing nearby rock caverns and access tunnels were mapped in the same hillside in the Precambrian gneiss. Good rock exposures were available in the arch of a nearby swimming pool cavern, in the arch of a parallel cavern housing the changing rooms and in the nearby Telephone Exchange caverns. This mapping was done in Phase I before drill holes from the surface were available. Figure 3 shows the location of the swimming pool cavern in relation to the subsequently excavated Olympic Ice Hockey Cavern.

The Precambrian gneiss had a frequency of jointing perhaps more than in Norwegian basement rocks in general. However, the joints were generally irregular, rough walled and with quite large variations in dip and strike. The spacing of the more persistent jointing was often several metres. The general joint character was one of low persistence, moderate to marked roughness and without clay filling, i.e. potentially positive characteristics for large spans. However, there were many short, irregular joints in the more tectonized red gneiss, which were responsible for the moderate RQD values (later ascertained to be 67% on average). Foliation was poorly developed, but generally had a strike of approximately E–W with a dip of 35–55°.

The hillside 25–50 m above the planned roof of the cavern had a generally smooth relief without marked depressions or traces of weakness zones. However, there was a marked NE–SW, sub-vertical fault zone crossing the access tunnel portals 50–100 m from the rock caverns, and affecting the jointing locally.

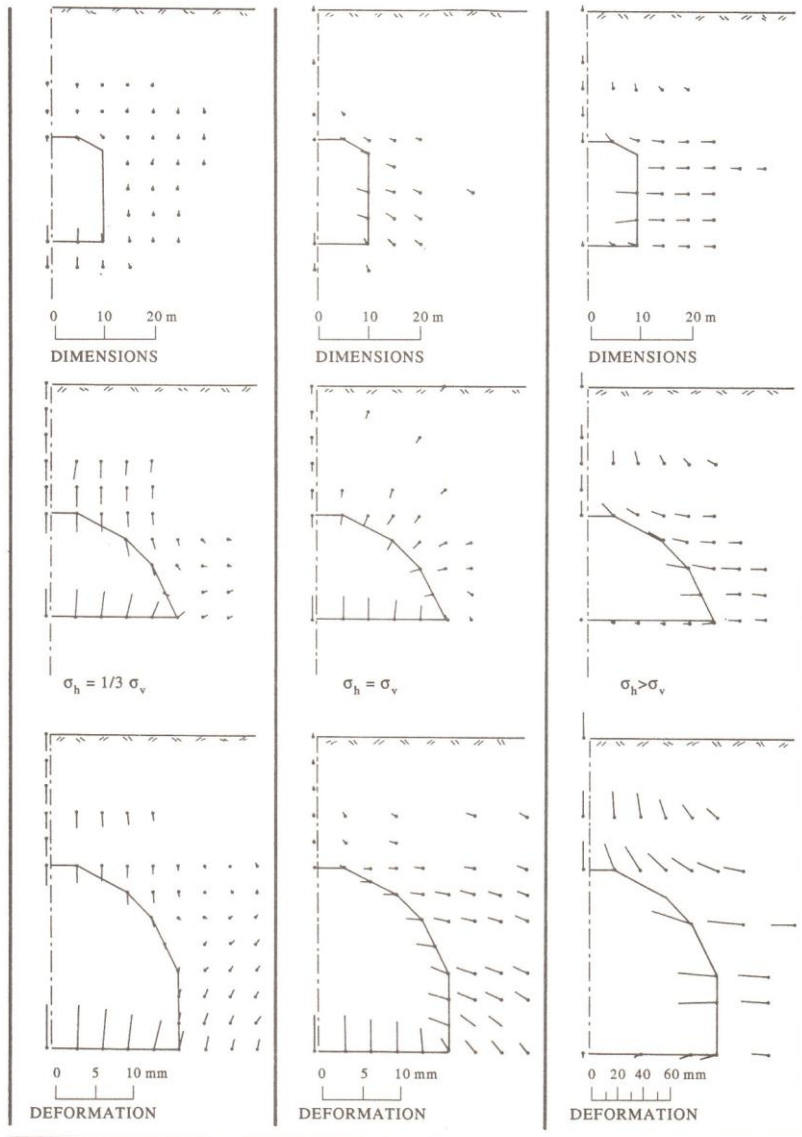


Fig. 1. Displacement vectors obtained from FEM continuum studies of large caverns [2].

The most typical rock mass quality actually visible in the existing caverns was the following:

$$Q = \frac{90}{6} \times \frac{2}{1} \times \frac{1}{1} = 30.$$

(RQD = 90%, two to three joint sets, smooth undulating joints, no alteration, little water in-flow, no stress problems.) The poorer quality rock could not be observed due to areas of shotcrete. Figure 4 (black histograms) shows the results of the *Q*-mapping in the existing

caverns during the Phase I studies. In general, the existing caverns were located between 25 and 100 m from the proposed site.

DRILL CORE ANALYSIS

In Phase II of the investigations, four diamond-cored holes of 50–70 m length were drilled by the Oslo consulting company, NOTEBY. Two holes were vertical and two were inclined at 45°, all of them

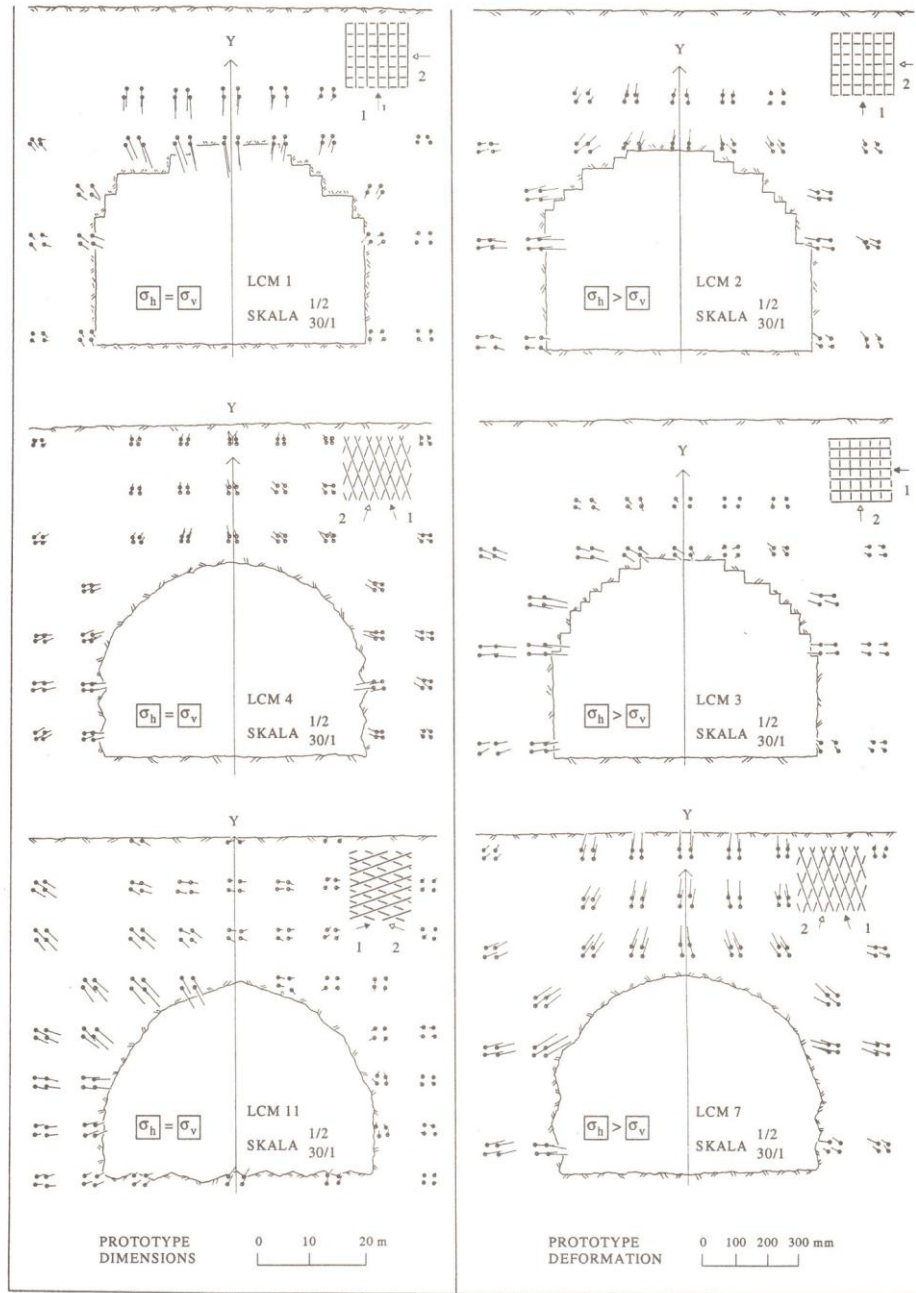


Fig. 2. Displacement vectors obtained from six physical models with jointing and stress levels as shown [2].

more or less within the potential 90×60 m footprint of the cavern, which in practice was nearer 100×100 m since the cavern orientation had yet to be finalized.

Analysis of the joints in the core indicated that a total of five different joint sets could be identified, but these seldom occurred in the same location, and jointing could also be described as sporadic. The most typical dip

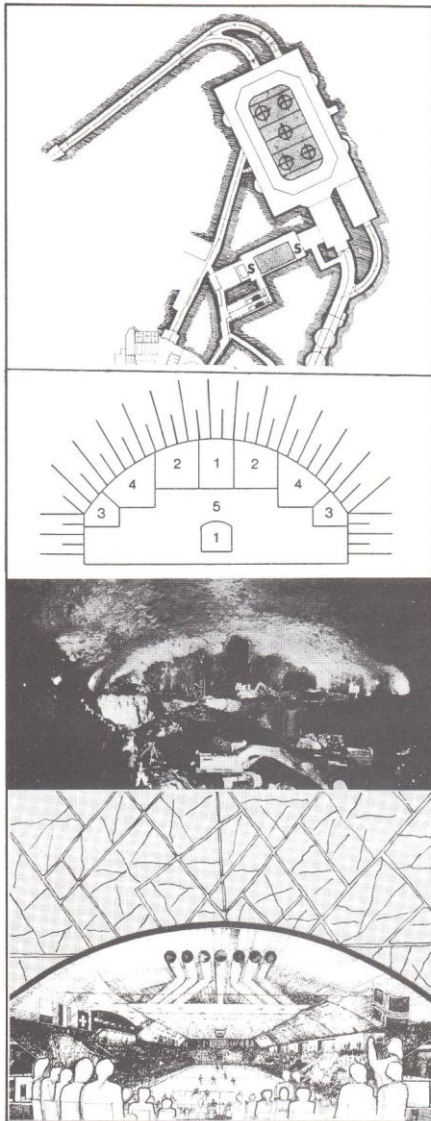


Fig. 3(a). Cavern layout, existing swimming pool (S), excavation stages, bolting pattern and construction.

angles were 50–65°, and some 40–45% of the joints showed this value. Some 25% of the breaks in the drill core were parallel to foliation, along diffuse planes of weakness. There appeared to be few through-going foliation joints, and their spacing was several metres. Some joints were healed due to mineralization. The most typical joint coatings or fillings were rust stains, epidote and quartz. Chlorite and calcite coatings occurred occasionally, while clay fillings appeared to be absent.

While part of the core showed evidence of minor brecciated or crushed zones of up to 0.5 m in thickness, no core loss or marked alteration was registered. In general, the joint frequency (F) was 4–8 per metre, but perhaps half the breaks in the core were due to diffuse weakness planes and not, technically speaking, joints. Through-going, well developed joints generally showed a frequency (F) of only 1–3 per metre. RQD was generally in the range 60–85%, though 15% of the core had an RQD = 100%. A large number of the joints had rough undulating surfaces, especially the foliation joints and the near-vertical N–S set of tension joints which probably paralleled the major principal stress.

ROCK MASS CLASSIFICATION

As part of the quality control procedures, the first application of the Q -system in the existing rock caverns, and the second application using the drill core were carried out by different engineering geologists. As indicated in Fig. 4, the two independent assessments were similar. Important minor differences were the observations of some poorer quality rock and coated joints in the drill core logging. Such areas were presumably coated with shotcrete which hindered observation in the cavern mapping.

Based on the combined cavern mapping and core logging the following typical rock qualities were expected in the Olympic Ice Hockey Cavern.

(1) Typical best quality

$$Q = \frac{90}{6} \times \frac{2}{1} \times \frac{1}{1} = 30.$$

(2) Typical poorest quality

$$Q = \frac{30}{9} \times \frac{1.5}{3} \times \frac{0.66}{1} = 1.1.$$

The weighted average, obtained from analysis of the complete set of histograms in Fig. 4, indicated the following:

(3) Weighted average

$$Q = \frac{73}{6.6} \times \frac{2.2}{1.8} \times \frac{0.9}{1.0} = 12.2.$$

Figure 5(a) shows the planned 60 m span ice hockey cavern plotted on the 1986 Q -system rock support diagram that was presented by Grimstad *et al.* [3]. The exceptionally large span and the high safety requirement (ESR = 1.0–0.8) placed the cavern right at the top or even above the available database. The latest update of the Q -system with some 1050 new case records [4] is shown in Fig. 5(b) for comparison. (The change of gradient on the new diagram accommodates the Gjøvik cavern case record.)

The need for careful numerical analysis to support the 1990 empirically derived reinforcement prediction was evident. Distinct element analyses of the cavern construction using the UDEC-BB code [5,6] are described later.

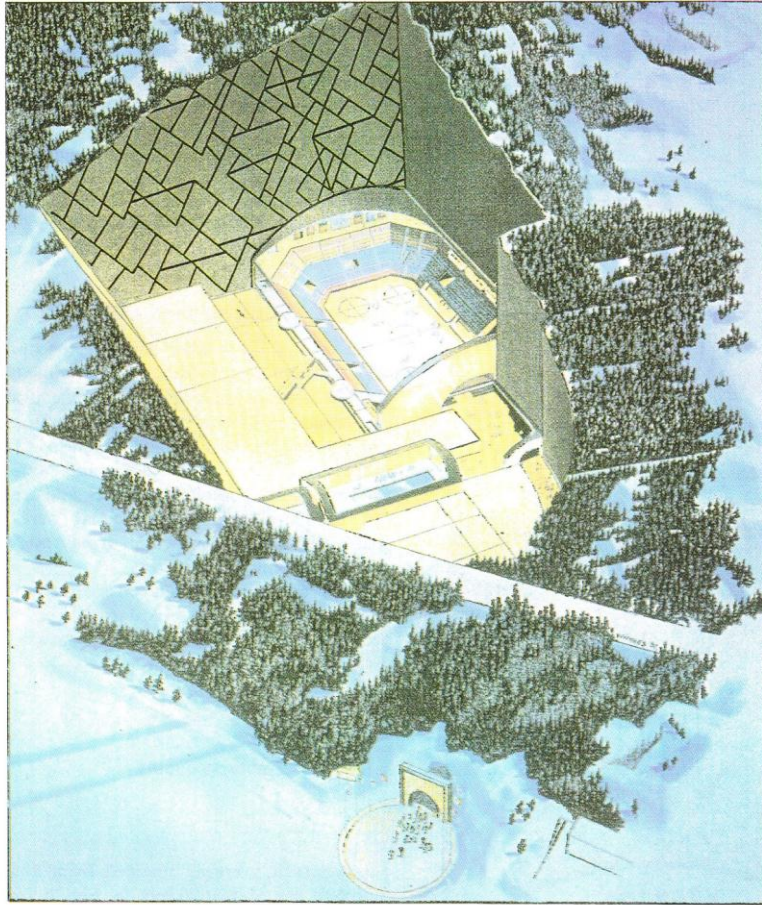


Fig. 3(b). Artist's three-dimensional view of cavern.

CROSS-HOLE SEISMIC TOMOGRAPHY

Important information for optimal siting and subsequent modelling of the cavern was obtained from NGI's exploratory cross-hole seismic measurements between vertical boreholes 1 and 3 (approximately 52 m apart) along the potential long axis of the cavern, and between borehole 3 and the 45° inclined borehole 2, along a section perpendicular to the potential axis [7]. The results of the tomographic analysis for these two profiles are shown in Fig. 6.

The *P*-wave velocity of the rock mass surrounding the cavern, which is located between 151 and 176 m.a.s.l., was generally in the range of 5000–5500 m/sec. In the first 20 m above the arch the velocity was somewhat reduced, lying generally in the range of 5100 down to

3700 m/sec, with the poorer quality some 10–20 m above the arch.

Detailed comparison between seismic velocity and the local RQD and joint frequency (measured along the drill core) demonstrated good correlation in the shortest vertical hole (No. 1, 45 m long). A velocity around 4000 m/sec at 15 m depth corresponded to an RQD = 60% and approximately 10 joints per metre. At 40 m depth, velocities of about 5000 m/sec corresponded to an RQD = 90% and 2 joints per metre. The latter corresponded to expected mid-cavern wall conditions (at 156 m.a.s.l.).

A feature of the results that has indicated good correlation between the prognosis and the excavated conditions is the reduced velocity and reduced rock quality predicted at the ends of the caverns. Subsequent

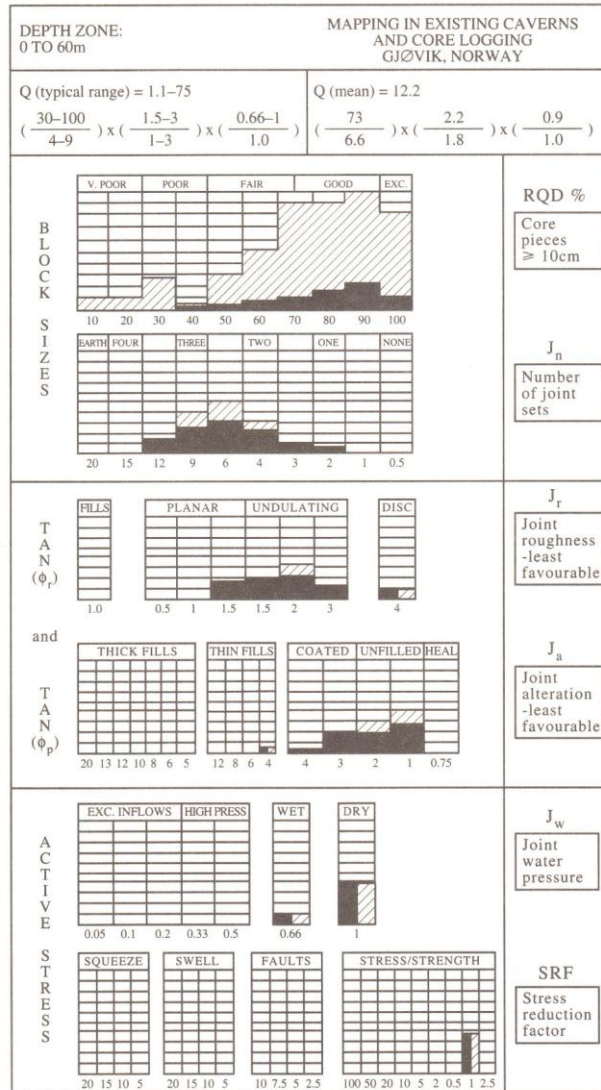


Fig. 4. Independent *Q*-system characterization in existing caverns (black). Combined database with four drill cores included (shaded).

Q-system mapping within the cavern indicated mean *Q*-values reducing from between 13 and 20 in the central areas to about 5 at the east end, and between 2 and 5 at the west end.

Detailed comparisons of the subsequently mapped *Q*-values in the cavern arch and *P*-wave velocity distributions obtained from the tomography indicated (for these jointed gneisses) the following approximate ranges:

$$Q = 5 \text{ to } 15, V_p = 3900 \text{ to } 4500 \text{ m/sec};$$

$$Q = 20 \text{ to } 30, V_p = 4700 \text{ to } 5200 \text{ m/sec}.$$

An approximately linear relation: $V_p = 50Q + 3600$ (m/sec) is indicated from these preliminary results over this limited range of rock qualities. Implications for future use are that tunnel or cavern support might be designed to some level of accuracy based on careful calibration of seismic surveys against rock mass classification.

Combination of the above near-surface data with *Q*-system application at other shallow sites [8] indicates that equation (1) may be a useful first approximation over a wide spectrum of near-surface rock qualities (and

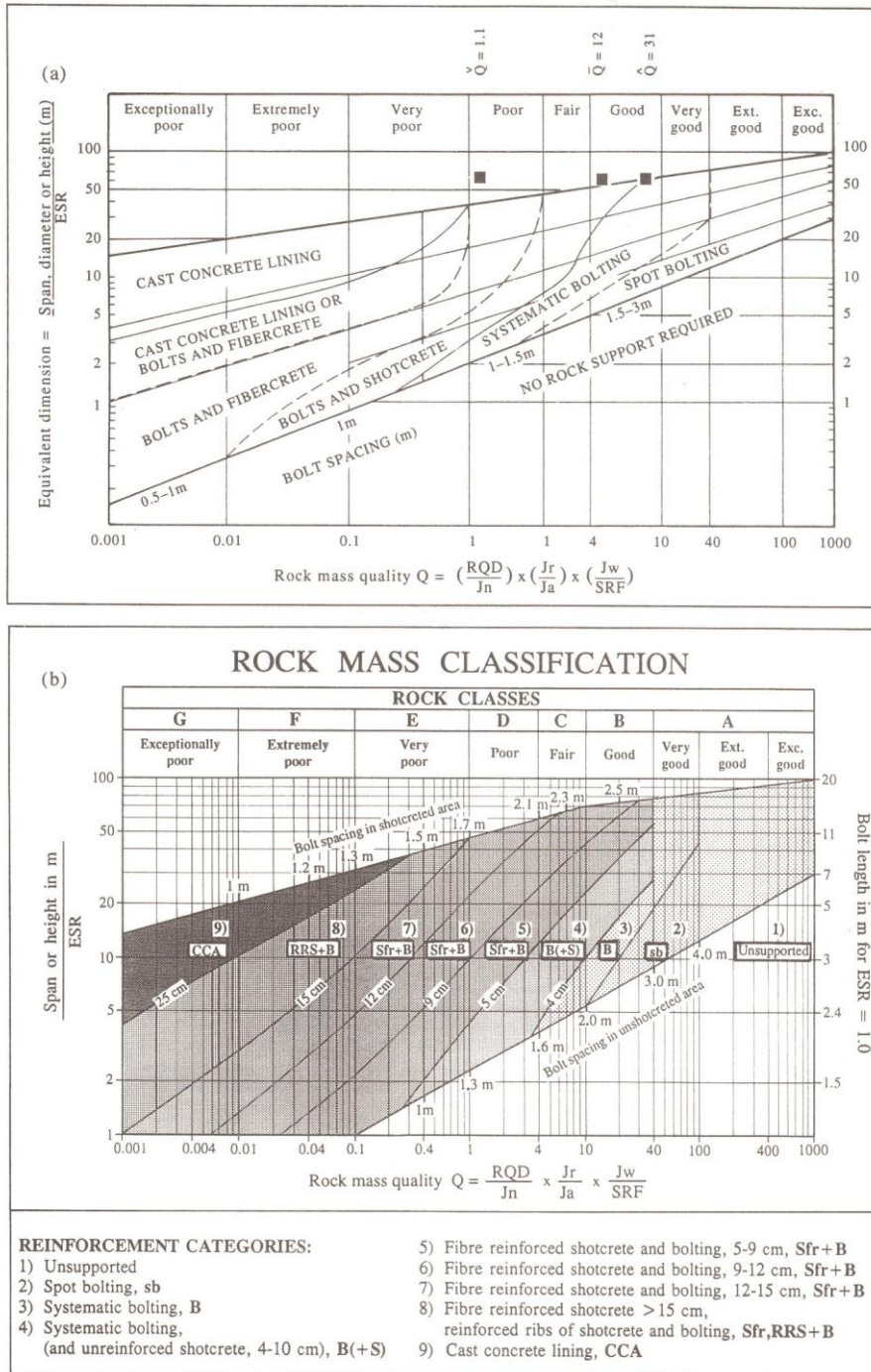


Fig. 5. (a) The 60 m span places the Olympic Ice Hockey Cavern at the top of the original *Q*-system reinforcement database [3]. (b) Updated *Q*-system diagram for NMT support design [4].

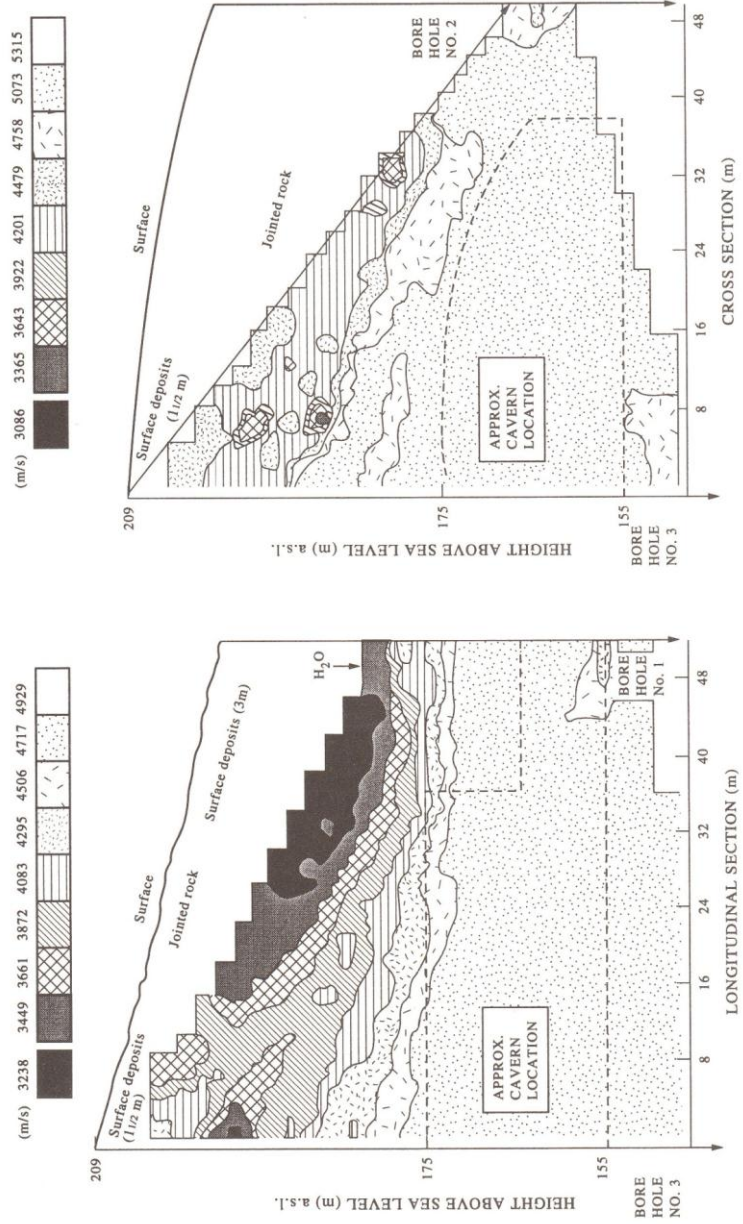


Fig. 6. Cross-hole seismic tomography for longitudinal and perpendicular cross-section through the cavern site.

stress levels). Data from projects in Norway, Sweden, Hong Kong and China include fault zone breccia, clay inter-bedded sandstones, siltstones, thin and thickly bedded sandstones, moderately and heavily jointed gneiss and granites:

$$V_p = 1000 \log Q + 3500 \text{ (m/sec)}$$

$$Q = 10^{\frac{V_p - 3500}{1000}} \quad (1)$$

The simple, easy-to-remember form of these results is shown in Table 1. Since the mean value of the deformation modulus is given by the approximation $E = 25 \log Q$ (see Barton [9]), combining this expression with equation (1) suggests that the rock mass deformation modulus can be estimated from:

$$E_{\text{mean}} = \left(\frac{V_p - 3500}{40} \right) \text{ (GPa)} \quad (2)$$

for values of P -wave velocity in excess of 3500 m/sec.

ROCK STRESS MEASUREMENTS

Preliminary measurements of rock stress using overcoring were performed by the Trondheim research organization SINTEF, utilizing a single short hole drilled from an existing cavern. These Phase I measurements indicated a surprisingly high horizontal major principal stress of about 4 MPa with an E-W orientation. However, these first measurements were carried out very close to an existing cavern.

Subsequent hydraulic fracturing and hydraulic jacking measurements carried out in Phase II by NGI confirmed the generally high horizontal stress levels, but suggested an N-S principal stress orientation (N 170° E), which was consistent with the N-S set of vertical tension joints and Permian dykes in the Oslo-Region to the south.

Due to the frequency of jointing in the upper 30 m or so of both holes, no measurements were initially

Table 1. Approximate correlation between Q and P -wave velocity

V_p (m/sec)	1500	2500	3500	4500	5500	6500
Q	0.01	0.1	1	10	100	1000

recorded more than 8 m above the arch. The major horizontal stress was estimated to be 3.5 MPa, 5 m above the arch of the planned cavern, and oriented N 174° E (approximately N-S). The intermediate stress estimated from joint jacking tests was estimated to be 2.0 MPa, 5 m above the arch, and oriented N 084° E (approximately E-W). The vertical stress was calculated to be approximately 1.0 MPa at this same location, some 40 m beneath the surface.

Shortly before cavern construction commenced in April 1991, NGI performed a further set of hydraulic fracturing stress measurements in the upper 30 m of rock. The combined data sets are shown in Fig. 7. The high stress to within about 10 m of the surface is a very positive aspect of the site for ensuring the stability of large span excavations.

It should be noted, however, that the stress is not as high as assumed in NGI's earlier studies of nuclear power plant caverns, as described in the Introduction. In one of the theoretical cases studied, a significant stress intercept at the surface was modelled, which allowed cavern heave to be predicted.

INPUT PARAMETERS FOR NUMERICAL MODELLING

(a) Young's moduli and uniaxial strengths

As part of the overcoring stress measurements performed by SINTEF in the Phase I studies, the E modulus and Poisson's ratio of the rock were measured. Mean values were $E = 51.5$ GPa, $\nu = 0.21$. According to tests on six 61 mm diameter samples the unconfined compression strength varied from 63 to 94 MPa reflecting the tectonized nature of the gneiss. In FEM studies performed by NOTEBY, rock mass moduli of 10, 30 and

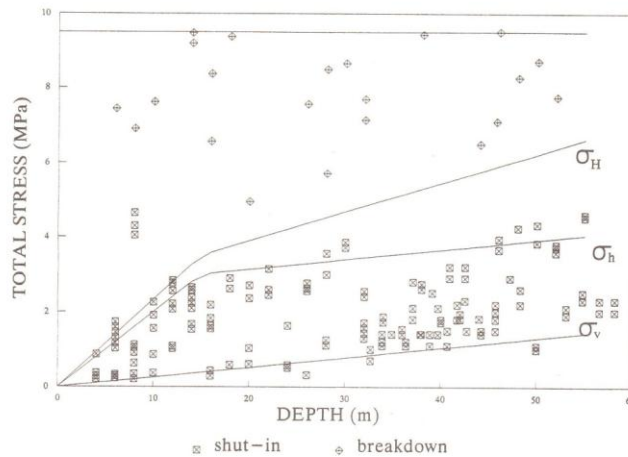


Fig. 7. Results of rock stress measurements using hydraulic fracturing and joint jacking.

51.5 GPa were utilized. Maximum predicted arch deformations with 28 and 48 m overburden ranged from 20.4 to 1.6 mm with the above range of moduli. Maximum horizontal stresses were mostly in the range 3–5 MPa. A similar range of stresses was seen in SINTEF's BEM computations.

(b) *Deformation moduli*

In the Phase I studies, NGI utilized both the Q -system and the RMR method [10] to estimate the rock mass deformation modulus (see Barton [9]). The estimated range of values was approximately 10–50 GPa, with an average of 30 GPa. This value was used in Phase I UDEC-BB calculations. However, in Phase II, the deformation modulus was estimated to take mean values of 20, 30 and 40 GPa, in three increasingly deep zones, as interpreted from drill core and seismic tomography results.

(c) *Shear strength parameters for the joints*

Joint roughness profiles were measured along 1 and 2 m long joint surfaces in the existing rock caverns, and gave an approximate indication of large scale waviness, with average (i) values of about 6° . The smaller scale features of joint roughness were recorded by roughness amplitude measurements and by performing tilt tests on some of the 101 joints recovered in the four drill cores. The most typical value of JRC_o (joint roughness coefficient, laboratory scale) was about 7.0. When corrected for block-size (approximately 0.5 m estimated *in situ*) the large scale value of JRC_n was 5.2.

The following assumptions were made concerning the peak friction angles for joints with small scale roughness (without undulations) and for joints with large scale roughness (with undulations that could not be sheared through) (see Barton and Bandis [11]):

(1) Laboratory scale

$$\phi_L = JRC_o \log \frac{JCS_o}{\sigma_n} + \phi_r \quad (3)$$

(2) Field scale

$$\phi_F = JRC_n \log \frac{JCS_n}{\sigma_n} + \phi_r + i \quad (4)$$

where σ_n is the effective normal stress.

Input parameters for the Barton–Bandis (BB) joint behaviour sub-routine that is used in NGI's version of Cundall's distinct element two-dimensional code (UDEC-BB) were as follows (see Makurat *et al.* [6]):

$$JRC_o = 7.5 \quad \sigma_c = 100 \text{ MPa} \quad L_n = 0.5 \text{ m}$$

$$JCS_o = 75 \text{ MPa}$$

$$\phi_r = 27^\circ$$

$$i = 6^\circ.$$

With these input data, a BB-Lotus model was used to produce graphical presentations of shear stress, displacement and dilation behaviour (Fig. 8) and normal stress-closure behaviour (Fig. 9). These and other BB-plots

were subsequently used to interpret the graphical output from UDEC-BB; for example the importance or otherwise of 1 or 2 mm of joint shearing; has the particular wedge-shaped block reached peak strength; has dilation started; is the hydraulic joint aperture reasonable, etc.?

UDEC-BB MODELLING (PHASE I)

A simplified joint geometry was assumed in the first phase of two-dimensional scoping exercises, based solely on joint mapping performed in the existing caverns. Core was not available, and over-coring stress measurements were assumed to be optimistically high due to nearness to an existing cavern. For this reason, a range of horizontal stress levels was assumed ($k_o = \sigma_h/\sigma_v = 0.5, 1.0$ and 3.0). Two conjugate sets of jointing of limited length were assumed as approximately representative of the observed jointing.

Stresses and displacements following completed (three stage) excavation of the 60 m span simulated cavern are as shown in Figs 10 and 11. Table 2 indicates maximum deformations for the three stages of cavern excavation, with the three levels of assumed horizontal stress discussed above.

The very positive effect of high horizontal stress levels and the equally negative effect of low horizontal stress levels were clear from these preliminary runs, and confirmed earlier physical models and FEM studies reported by Barton and Hansteen [2]. Under certain conditions of cavern dimension, thickness of arch, horizontal stress level and joint orientation, heave of the arch will occur. The ideal for minimizing joint shearing might appear to be a design more or less "in balance" between downwards and upwards oriented deformation. However, slight joint shearing (to mobilize resistance) might be considered even more advantageous. In view of the very large span, the 4 mm of deformation recorded with $k_o = 3$ to 4 must be considered nearly ideal.

The large deformation (19.2 mm) recorded in the model with lowest k_o was caused primarily by major joint shearing on the right-hand side of the two wedges in the arch. This movement stabilized due to joint dilation and build-up of normal stress, despite lack of modelled bolting in these preliminary studies.

UDEC-BB MODELLING (PHASE II)

The second phase of UDEC-BB modelling was performed following the core drilling, stress measurement and cross-hole seismic tomography. Input data were therefore more refined. However, the number of excavation stages was still limited, since no final designs were yet developed for the cavern. There was still no significant funding for the cavern project.

The horizontal stress distribution, joint pattern and general input data used in Phase II studies with UDEC-BB are illustrated in Fig. 12. Two models were run, the first with 25 m of overburden, the second with 45 m of overburden, to represent different vertical cross-sections. Only three excavation stages were modelled in each case.

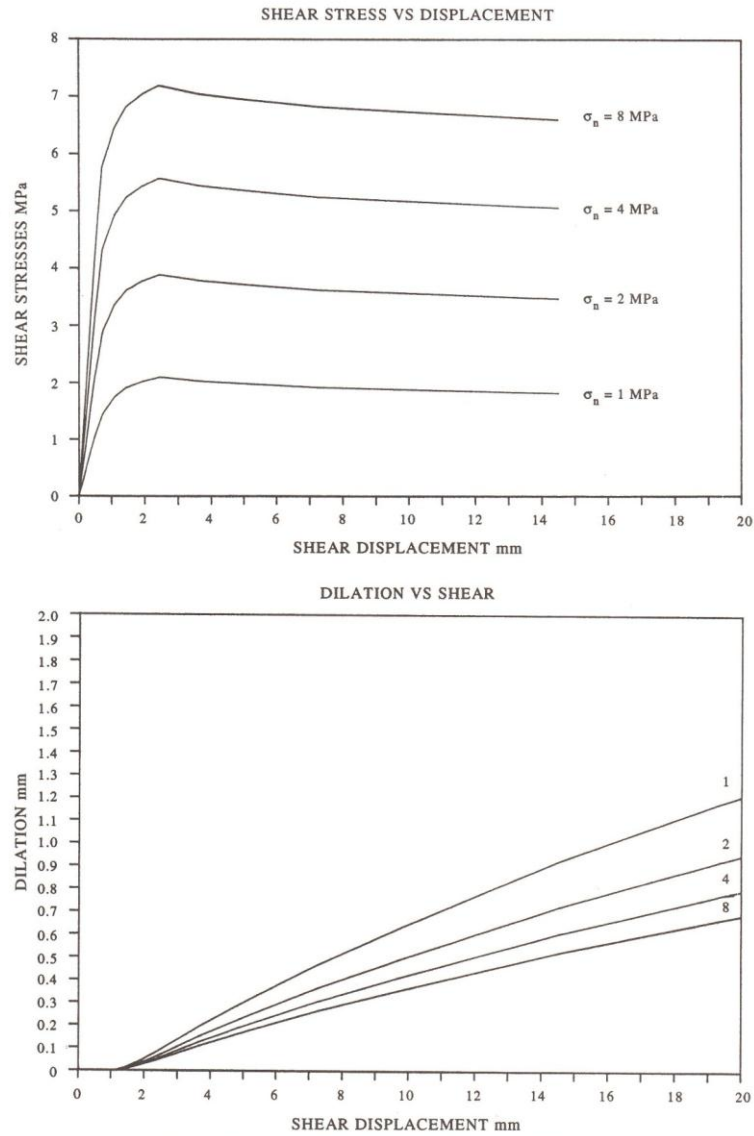


Fig. 8. Shear stress-displacement-dilation prediction from BB joint model.

The assumed level of horizontal stress used in Phase II modelling lies close to the major stress line presented in Fig. 7. While this may appear a non-conservative assumption, it is supported by hydraulic fracturing stress measurements of 4.0 and 2.6 MPa at an elevation of 150 m.a.s.l., and by overcoring measurements of 4.3 and 3.4 MPa for major and intermediate stress at the same elevation (with uncertain excavation effect). A number of shut-in tests using joint jacking gave values of

3.0 MPa as high as an elevation of 180 m.a.s.l. Favourable horizontal stress levels are therefore apparent along both axes.

Graphical presentation of the UDEC-BB results will only be given for Model II which had the maximum overburden of 45 m. However, results for Model I (25 m depth) will also be given in tabular form, so that comparisons between the two depths can be made.

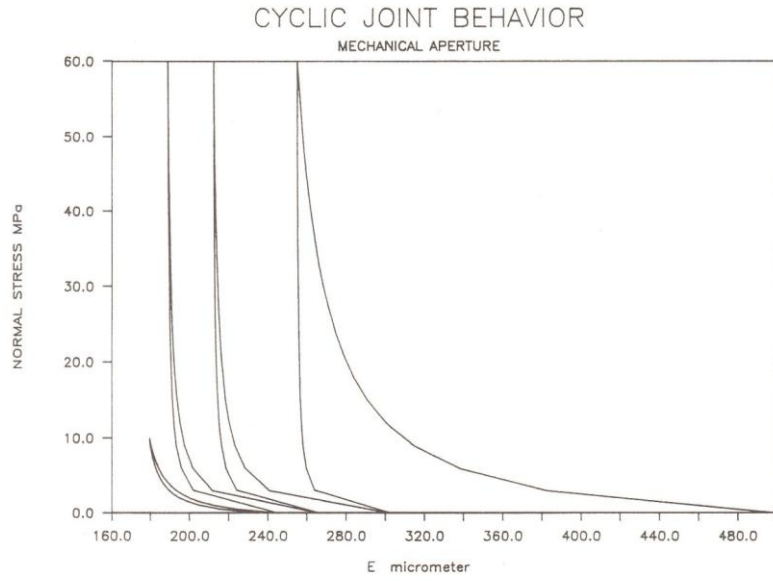


Fig. 9. Normal stress-closure prediction from BB joint model.



Fig. 10. Simplified Phase I UDEC-BB runs. Principal stresses with $k = 0.5, 1$ and 3 .

Fig. 11. Simplified Phase I UDEC-BB runs. Deformation vectors with $k = 0.5, 1$ and 3 (maximum = 19.2 mm).

Table 2. Maximum deformations recorded in Phase I UDEC-BB studies, with simplified jointing and only three excavation stages

Cavern dimensions (m)	$k_0 = 0.5$ (mm)	$k_0 = 1.0$ (mm)	$k_0 = 3.4$ (mm)
20 × 10	0.64	0.61	0.65
60 × 10	19.5	4.2	3.7
60 × 20	19.2	8.4	4.0

(a) *Stress distribution caused by excavation*

Figure 13 illustrates the redistribution of stresses caused by the three stages of excavation. Relatively stress-free blocks are evident in the immediate proximity to the arch. In practice such blocks would be secured by the systematic rock bolting. Smaller scale versions of the same phenomenon would be secured by the shotcrete, which was wet process, steel fibre reinforced (i.e. an important component of NMT support, which is ideal for jointed rock that is prone to overbreak).

(b) *Deformation caused by excavation*

Figure 14 illustrates the modelled deformation that occurs as a result of the three stages of numerical excavation. Table 3 summarizes the maximum deformations recorded (in mm) for the three excavation stages, both for Models I and II (25 and 45 m overburden). Results are similar to those obtained with simplified models in Phase I, for the cases with $k_0 = 1$, and for $k_0 = 3$ to 4.

Maximum deformations of about 2 mm in the first stages of excavation are caused by gravitational (and perhaps stress driven) instability of two wedge-shaped blocks in the arch. These stabilized after about 1.5–2.0 mm shear, due to the dilation that occurs on the simulated non-planar joints. The BB-Lotus model of joint behaviour (Fig. 8) predicted peak friction mobilization after about 2 mm of dilatant shear with the assumed block size (0.5 m). This dilation mechanism was clearly operative in the joint sub-routine in UDEC-BB (and generally also is in practice when there is significant joint roughness).

The very small deformations calculated with both models suggests that the modelled depth, span, stress conditions and joint character are favourable for the very large span.

(c) *Shear deformation along joints caused by excavation*

The relatively complicated behaviour of a jointed rock mass (even in two-dimensions) is quite well illustrated by the successive developments of joint shearing seen in Fig. 15. Maximum values for both Models I and II are listed in Table 4.

Marked shear deformation was evident along the joints defining the wedge-shaped blocks referred to earlier. However, the maximum joint shearing magnitudes (3.2–3.4 mm) were experienced along the assumed horizontal joints at each side of the arch, once these were

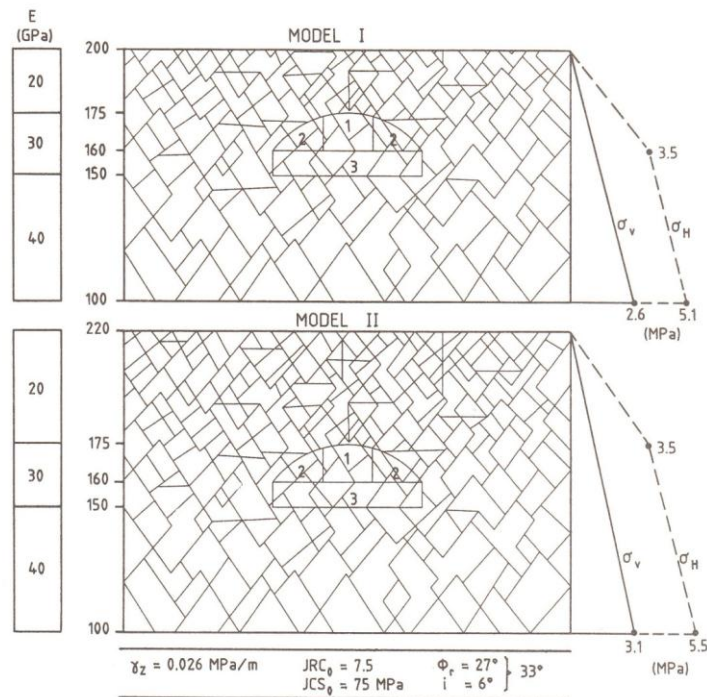


Fig. 12. Phase II assumptions concerning boundary stress conditions, deformation modulus (E) and joint properties. Model I = 25 m overburden, Model II = 45 m overburden.

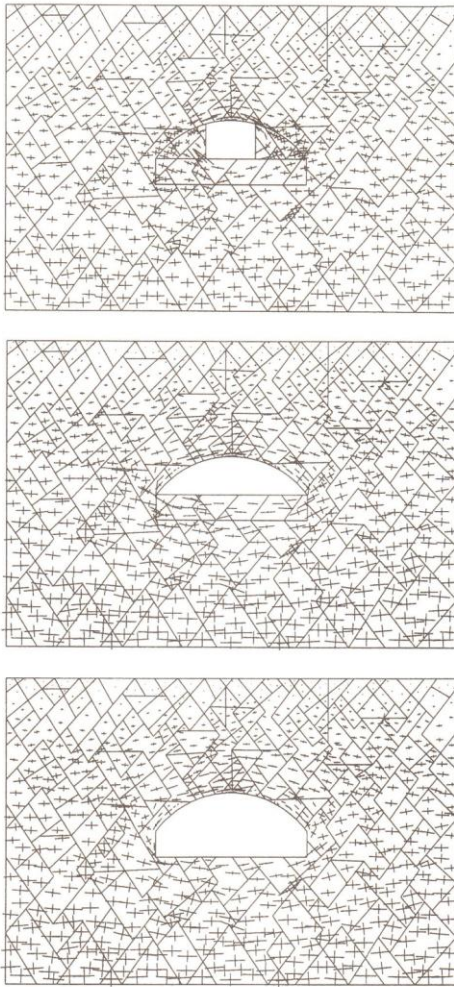


Fig. 13. Phase II UDEC-BB runs for Model II: principal stresses.

exposed by excavation. The third stage of excavation (benching downwards by 10 m) caused almost a five-fold increase of these particular shear displacements, which would be resisted in practice by the systematic bolting of the arch and haunches. Slight shear deformations (small fractions of the order millimetres) were registered right up to the surface, even in the model with 45 m overburden. Again, these would tend to be minimized if systematic numerical bolting had been applied. (See Phase III modelling for results of bolting.)

(d) Joint conducting apertures

Other graphical output from the UDEC-BB modelling indicated the locations and magnitudes of enhanced joint conducting aperture from which rock mass permeability could be deduced. Enhancement of

permeability generally occurred in the axial direction, due to block displacement effects at quite a large number of joint intersections. Small, rectangular channels formed at these locations had maximum apertures ranging from 1.2 to 1.9 mm, compared to the initial, stressed hydraulic joint apertures of about 24 μm .

UDEC-BB MODELLING (PHASE III)

(a) Introduction

During cavern construction, which started in April 1991 and finished in December 1991, NGI's role was one of research co-ordinator of rock mechanics and engineering geology. NOTEBY, as consultants, had responsibility for the day-to-day decisions on geology and rock support. The opportunity was provided for NGI to

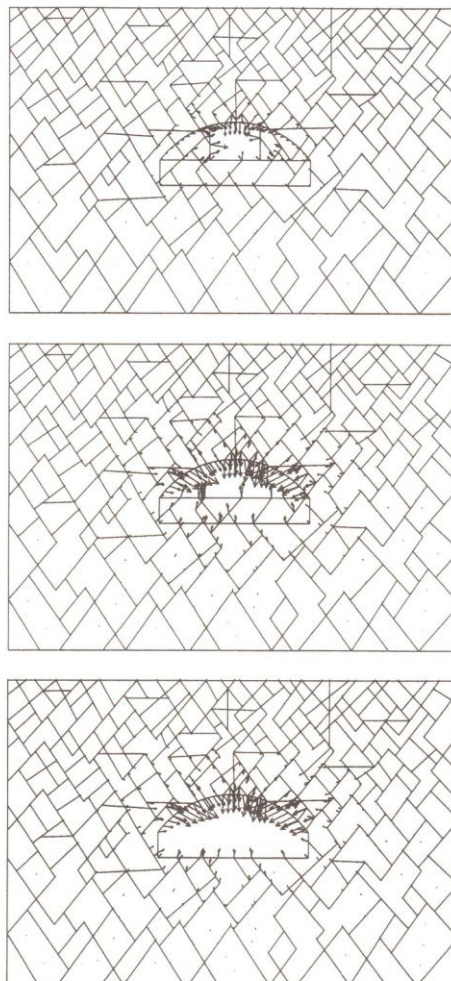


Fig. 14. Phase II UDEC-BB runs for Model II: deformation vectors (maximum 4.8 mm).

Table 3. Summary of maximum deformations (mm)

Model No.	Overburden (m)	Cavern dimensions (in m × m)		
		20 × 15	60 × 15	60 × 25
I	25	1.8	2.0	4.8
II	45	2.4	3.8	5.3

Table 4. Summary of maximum joint shear deformations (mm)

Model No.	Overburden (m)	Cavern dimensions (in m × m)		
		20 × 15	60 × 15	60 × 25
I	25	1.5	1.9	3.4
II	45	2.0	2.8	3.2

perform detailed geotechnical mapping of the actual stages of excavation, and also to model the predicted influence of three new adjacent caverns, which were subsequently excavated between January and April 1992, for the Norwegian Postal Services.

The UDEC-BB model geometry used in the third phase of modelling is shown in Fig. 16. Phase III modelling was also predictive (Class A); the same basic joint geometry, input data and boundary stress

conditions were applied to the Phase III model as those shown in Fig. 12 (Phase II), i.e. no attempt was made to back-calculate to obtain improved input data. A diagram of the bolting pattern and excavation sequence that was modelled is shown in Fig. 17.

(b) Bolt reinforcement

The numbers within the cavern in Fig. 17 refer to the excavation steps. The rock mass in the cavern arch and the walls was numerically reinforced by untensioned fully grouted rock bolts and untensioned fully grouted cable anchors after each numerical excavation step.

The permanent bolting in the arch consisted in general of alternate 6 m rebar bolts and 12 m twin-stranded cables in a 2.5 × 2.5 m and 5.0 × 5.0 m pattern. The former had a diameter of 25 mm and a yield capacity of 22 tons, while the latter had a diameter of 12.5 mm and a capacity (for each strand) of 16.7 tons at yield.

With the exception of the cables, the rock reinforcement principles were generally typical of those used on major NMT projects (see Barton *et al.* [8]). The 6 m bolts and some temporary bolts were placed before the 12 m cable bolts in both the 10 m span pilot tunnel arch and in the primary 35 m span top heading. Five centimetres of steel fibre reinforced shotcrete was sprayed first, followed by another 5 cm to make the final 10 cm thickness. The shotcreting was by the wet process, using 50 kg/m³ of 25 mm EE steel fibres, with a concrete quality of 35 MPa. The fibre reinforced shotcrete has not been modelled numerically, due to the uneven blasting profile caused by unavoidable overbreak on the three to four joint sets, despite smooth wall blasting designs.

Considering both the arch and walls together, a total of 194 × 12 m long cable bolts were set in the arch, and 66 × 10 m long cable bolts were set in the walls. In addition, a total of 1174 CombiCoat corrosion-protected 6 and 5 m long bolts were set in the arch and walls plus 845 × 3 and 4 m long temporary bolts and 1068 m³ of fibre reinforced shotcrete. The cavern surface area covered by the shotcrete was approximately 10,000 m².

In the UDEC-BB model, each of the excavation steps was first run to equilibrium without any use of reinforcement. When 100% of deformation was achieved, the point where approximately 50% of this deformation had occurred was used as the starting point for bolt installation, using save-files. This was done in an attempt to allow for the elastic deformation that would have already occurred before bolt installation, at the current excavation face.

(c) Stress redistribution caused by excavation

The UDEC-BB results for each of the excavated steps are given in Table 5. The redistribution of stresses that

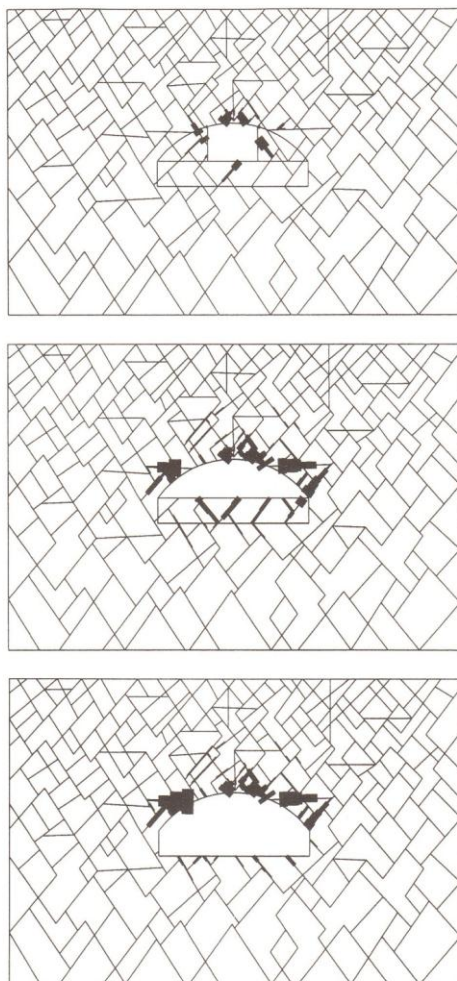


Fig. 15. Phase II UDEC-BB runs for Model II: joint shearing magnitudes (maximum 3.4 mm).

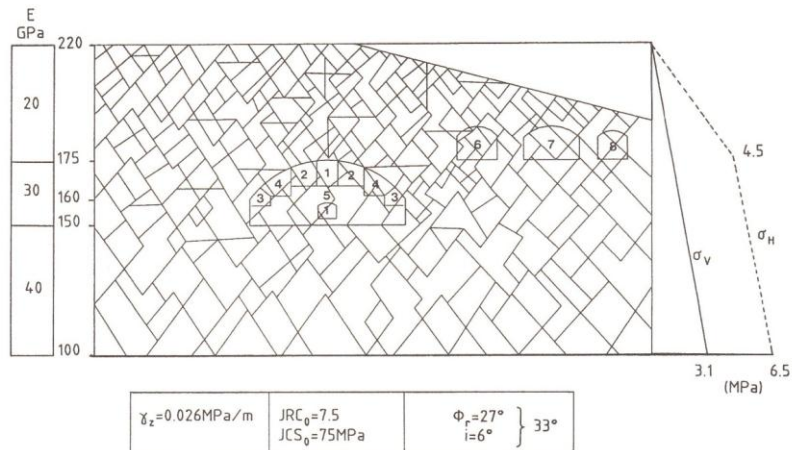


Fig. 16. Phase III UDEC-BB model, showing additional Postal Service caverns. Distribution of deformation moduli and boundary stresses are shown.

occurred between the fourth and fifth excavation step are shown in Fig. 18.

In the arch of the cavern, some nearly stress free blocks can be observed. These blocks would have been secured in practice by the systematic rock bolting. Shotcrete (fibre reinforced) which was not modelled in this study, would have secured the smaller blocks, representing the detailed joint structure.

(d) Displacements caused by excavation

Detailed results of displacement development at each stage of excavation are given in Table 5. In the centre of the Olympic cavern arch, the maximum downward displacement at Stage 5 was 4.33 mm. This increased slightly with each Postal Services cavern excavation, especially with the last. Figure 19 shows this development rather clearly. Presumably, the excavation of adjacent caverns gradually reduced the horizontal stress levels and allowed greater arch displacement. This effect was predicted by NGI prior to the decision to excavate the adjacent caverns, which fortunately were excavated at a fairly high level relative to the stress arch of the Olympic Ice Hockey Cavern.

This case record throws light onto an interesting dilemma as to the “rights” to surrounding rock (and accompanying stress arch) of a previous cavern project. A new cavern owner’s subsequent rights to excavation in the adjacent rock mass may need to be limited, based on appropriate modelling predictions.

(e) Bolt load development

Figure 20 illustrates the development of bolt loads for the 5 and 6 m systematic bolting of the walls and arch, and for the 10 and 12 m twin-stranded cable bolts. Note that there are some increases of bolt loading for the 6 m

bolts caused by excavating the final Postal Services cavern. There are also one or two slight decreases in load.

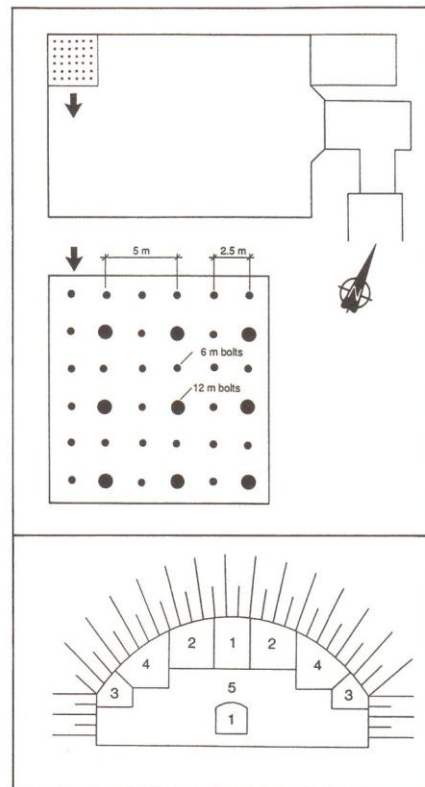


Fig. 17. Bolting pattern and excavation sequence [13].

Table 5. Summary of Phase III Gjøvik Ice Hockey Cavern modelling (with Postal Service caverns as steps 6, 7 and 8 of excavation)

Modelled parameter	Olympic cavern					Postal caverns		
	Step 1	Step 2	Step 3	Step 4	Step 5	Excav. of 1st cavern	Excav. of 2nd cavern	Excav. of 3rd cavern
Max. stress (MPa)	9.29	11.5	9.91	8.39	8.37	8.56	8.71	8.83
Displacements (mm)								
● maximum	1.85	1.80	2.63	6.99	8.16	8.28	8.43	8.65
● wall	—	—	—	1.33	3.78	3.88	3.92	3.97
● crown (vertical component)	0.50	1.08	2.62	4.05	4.33	4.39	4.87	7.01

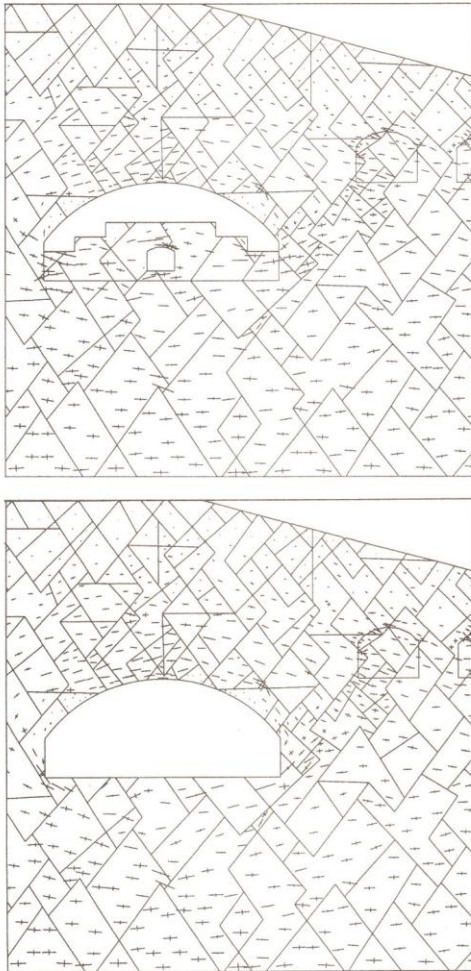


Fig. 18. Redistribution of principal stresses between the fourth and fifth excavation steps, Phase III.

DEFORMATION MONITORING AND COMPARISON WITH UDEC-BB RESULTS

NGI, NOTEBY and SINTEF were all involved in performance monitoring studies during the cavern construction. The near surface location of the cavern meant that extensometers could be placed in boreholes from the

surface using holes of 30–40 m depth. Figures 21 and 22 show the location of the MPBX extensometers (E1 to E6) which were installed prior to cavern construction, and reached 1.5 or 2 m above the cavern arch. E7 was NOTEBY's sliding micrometer instrument which confirmed the assumed, fairly uniform gradients of deformation.

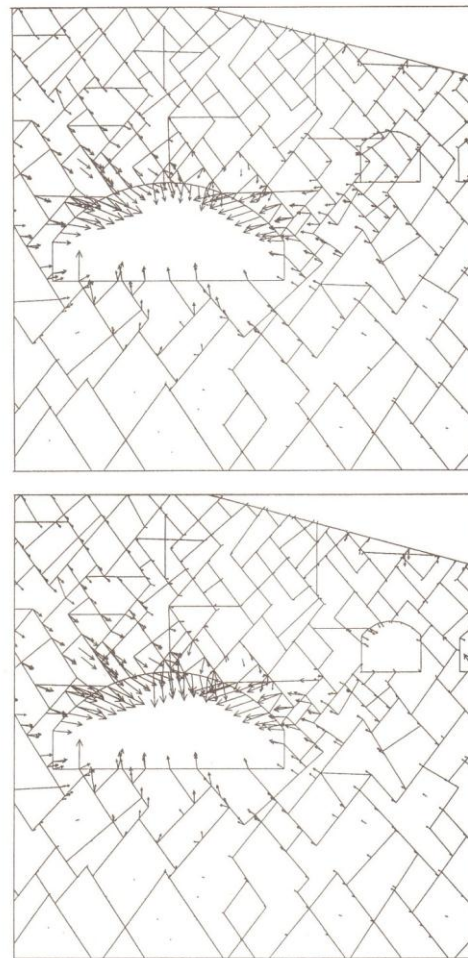


Fig. 19. Development of deformation vectors between the fifth excavation step and the excavation of the third Postal Service cavern.

Surface precision levelling was carried out at E1, E4 and E7 installations (above the cavern centre-line), and showed a gradual increase of subsidence to between 2.5 and 3 mm during the 4 months it took to excavate the full 62 m wide \times 91 m long \times 8 m high top heading. The initial deformations recorded by the six Interfels MPBX are shown in Fig. 23. Some initial episodes of slight heave (arching upwards) are seen adjacent to excavation faces due to the high stresses. The centre of the cavern (at the location of E4) had subsided at this stage approximately 3 mm relative to the surface 35 m above. The 3 mm had to be added to the surface subsidence of approximately 2.5–3 mm to obtain the preliminary net deformation.

A further source of deformation was the dilation of the blast-damaged zone within the cavern. SINTEF's twin anchor S1 to S3 extensometer bolts of 2 and 13 m

length were located in the arch behind the advancing face in the 80 m² pilot tunnel. They showed maximum vertical deformation values of 2.8, 1.3 and 2.9 mm.

To obtain the maximum vertical deformation of the centre of the arch, it is necessary to add E4 and S2 results to the maximum surface subsidence of approximately 4.5 mm. A value of 8.2 mm is obtained. The equivalent result at E1/S1 towards the SW end of the cavern is 7.0 mm, and towards the NE end (E7/S3) the result is 7.5 mm. [NOTEBY's sliding micrometer (E7) showed a total 2.23 mm of deformation over its 28 m length.] However, there is uncertainty concerning the sensitivity/accuracy of the surface subsidence measurements.

Figure 24 shows the cumulative results for the three sets of instruments located along the cavern centre-line. There has been no significant change to these values (i.e. ≥ 0.25 mm) at the time of writing (900 days).

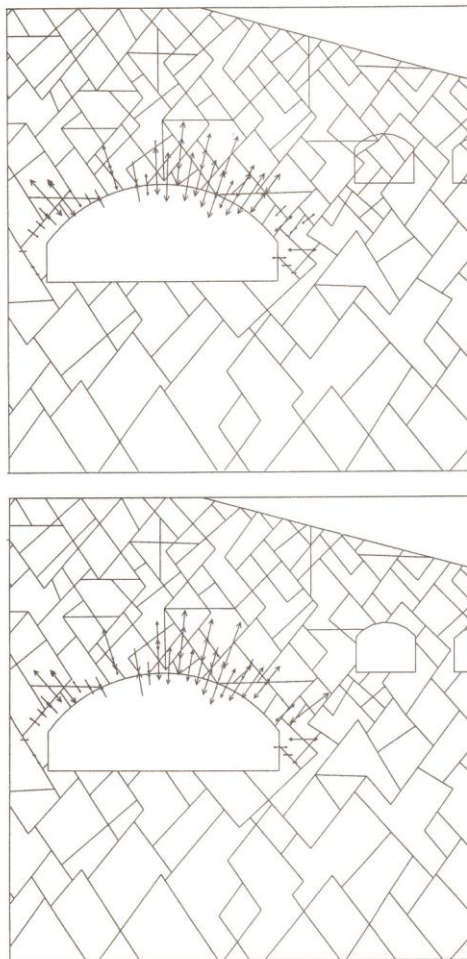


Fig. 20. Development of axial forces on the rock bolts between the fifth excavation step and the excavation of the third Postal Service cavern.

RMMS 31/6-E

ROCK MASS QUALITY IN THE CAVERN ARCH

During the core logging performed in the feasibility studies, the mean Q -value (12.2, Fig. 4) calculated by means of data from the four boreholes gave a slightly higher rock quality than that found during subsequent cavern mapping shown in Fig. 25 ($\bar{Q} = 7.4$ in pilot heading, $\bar{Q} = 9.4$ in cavern arch). This was probably due to the shotcrete covering poorer quality rock when the pre-existing caverns were mapped in 1990.

The rock exposed in the Olympic cavern was red and grey jointed gneiss of PreCambrian age. The average mapped RQD (rock quality designation) of 60–70% 12 represented only fair rock quality. The PreCambrian gneiss had a network of micro-joints and isolated zones with clay fillings.

The geotechnical investigations during the construction involved registration of rock quality using the Q -system. Detailed joint surveys in the excavated portions of the cavern also provided data on joint orientations, joint character and spacing. Measurements of strike and dip of the main discontinuities were made throughout the cavern. Data from 35 areas which together make up the majority of the upper part of the cavern were collected [12]. The relevant Q -values are shown in Fig. 21 (see numbers in squares). These confirm the lower quality of rock at the ends of the cavern, as seen in the cross-hole seismic tomography (Fig. 6).

(a) Geotechnical logging charts

Q -system data for rock mass classification, and joint descriptions to confirm distinct element (UDEC-BB) modelling input were recorded in histogram form, as shown in Fig. 26. Incorporating all the information in a PC-based spread sheet makes it possible to see the variation in the different parameters throughout the rock structure, and combine or separate adjacent data sets as desired.

The jointing in the cavern has proved to be irregular, rough walled and with quite large variations in dip and strike, more or less as predicted earlier. A photograph of

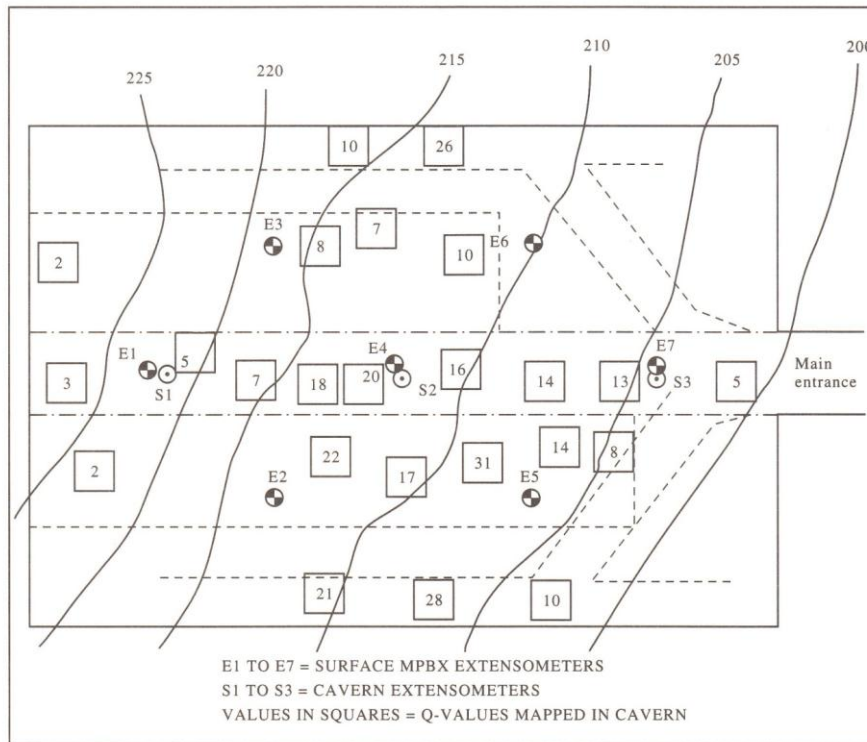


Fig. 21. Location of surface MPBX extensometers (E1 to E7) and cavern extensometers (S1 to S3) shown in relation to local rock mass Q -values (squares) as mapped in the cavern arch and access ramps.

representative jointing in the central bench area (N-side) is shown in Fig. 27. Although the 3 to 4 joint sets caused marked overbreak, the joint roughness together with the rather high horizontal stresses of about 3.5–4 MPa at a depth of 45 m below the surface (and perpendicular to the long axis of the hall) have been found to be very favourable for the stability of the cavern, and explain the rather small deformation magnitudes.

(b) *Displacements compared with Q -database*

The range of Q -values obtained in the cavern and the corresponding range of displacements recorded by the MPBX, provided data for comparison with earlier Q -system case records [15]. An updated plot of results for Q /SPAN (in metres) versus deformation is shown in Fig. 28, and includes Gjøvik cavern data measured during the various excavation stages.

In general, the results are on the low side, and emphasize the positive effect of the high horizontal stress. In retrospect, the mean Q -value for the top heading (7.4) and for the arch as a whole (9.4) could perhaps be adjusted upwards by a more favourable estimate of $SRF = 0.5$ (favourable high stress). This value is seen immediately to the left of the assumed histogram values of 1.0 shown in Figs 25 and 26.

CONCLUSIONS

- (1) An exceptionally large span (62 m) rock cavern has been constructed in rock varying from poor to fair to good quality. Mean Q -values observed in Phase I mapping prior to construction were 12, and the predicted range was 1–31. Mean Q -values observed in the cavern pilot tunnel of 80 m² cross-section were 7.4 (typical range 4–27), and in the cavern arch as a whole 9.4. The typical range observed here was 1–30, more or less as predicted.
- (2) Key properties favourable to large cavern construction have been the high horizontal stresses and the relative roughness or waviness of foliation planes and of the more continuous joints. The Norwegian method of tunnelling (NMT) type of permanent rock reinforcement, using steel fibre reinforced shotcrete and rock bolts, has taken care of less favourable features such as the less favourable joint orientations and mean RQDs of only 65–70% in the disturbed rock exposed by the blasting.
- (3) The usefulness of rock mass characterization, cross-hole seismic tomography and rock stress measurements has been demonstrated by the good definition of input data for forward prediction

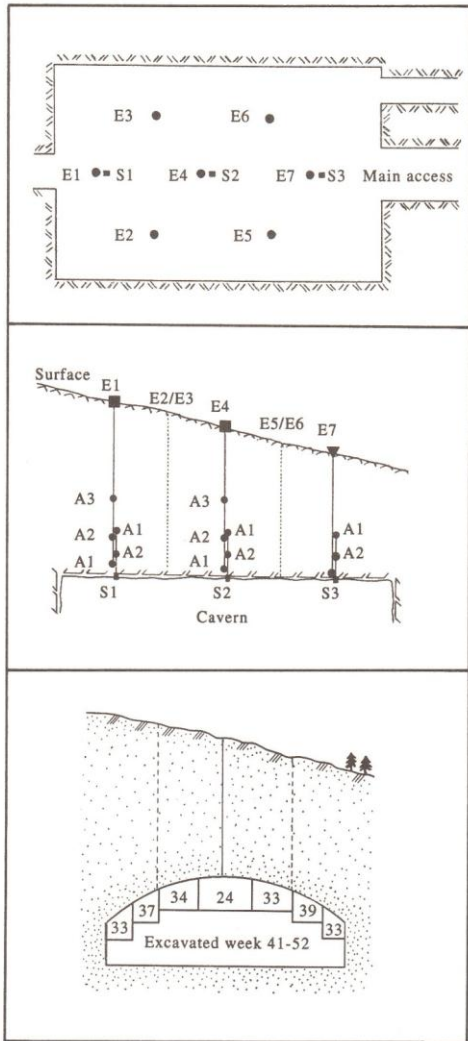


Fig. 22. Longitudinal and perpendicular cross-sections showing instrument locations [14].

(class A) modelling. Four different methods of deformation measurements have confirmed the relatively small deformations that were predicted by UDEC-BB to be as little as 5 mm (Phase II simplified model) and as large as 8 mm (Phase III, correct excavation sequence and adjacent caverns).

- (4) Precision levelling of the MPBX instrument heads at the surface, combined with deformation measurement throughout 30–40 m of rock overlying the cavern indicate maximum deformations

in the range 7–8 mm along the cavern arch centre-line.

- (5) The combination of high stress and shallow location place the cavern close to the balance point between upward and downward deformation as demonstrated by earlier physical models and FEM analyses.
- (6) The effective prediction of behaviour prior to cavern design, the efficient excavation and NMT rock reinforcement, and the continuous monitoring of behaviour provided confidence in the project and were instrumental in its completion ahead of schedule and within budget.

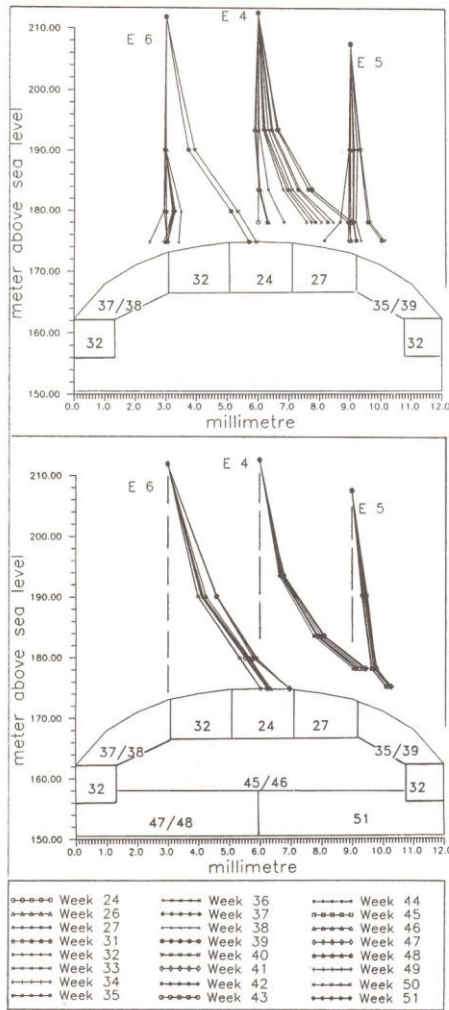


Fig. 23. Six MPBX installed from the surface prior to construction, monitored the weekly excavation. (Heave to the left, subsidence to the right.) Results for E4, E5 and E6.

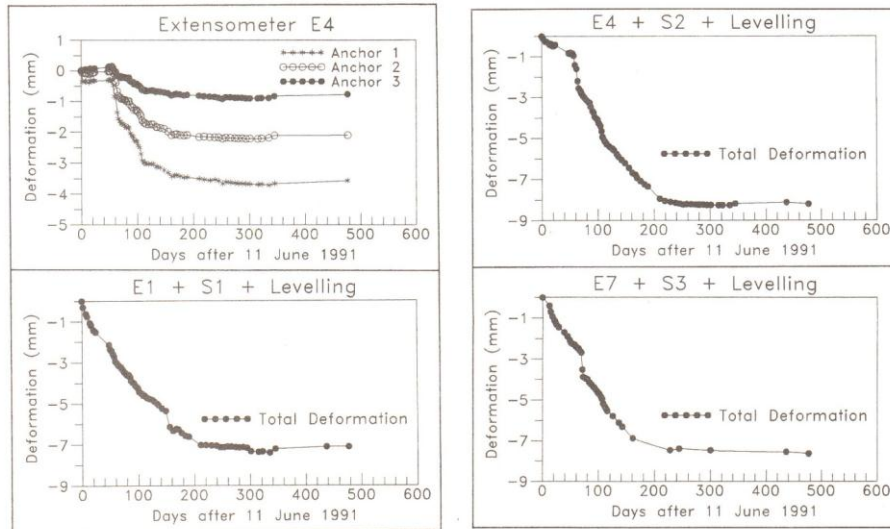


Fig. 24. Cumulative displacements along the cavern arch centre-line. The Olympic cavern was completely excavated at 200 days, the Postal Service caverns at 350 days (7.0, 8.2 and 7.5 mm = maximum centre-line displacements).

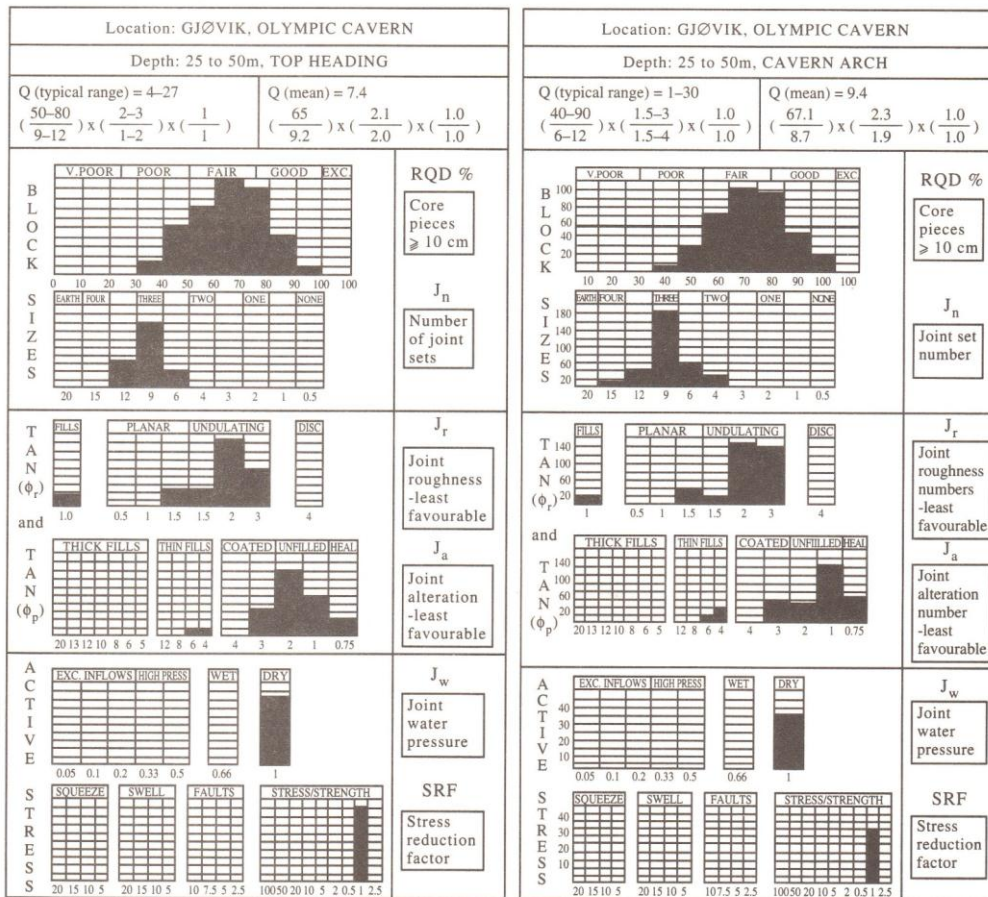


Fig. 25. Q-logging in the Olympic cavern top heading and arch [12].

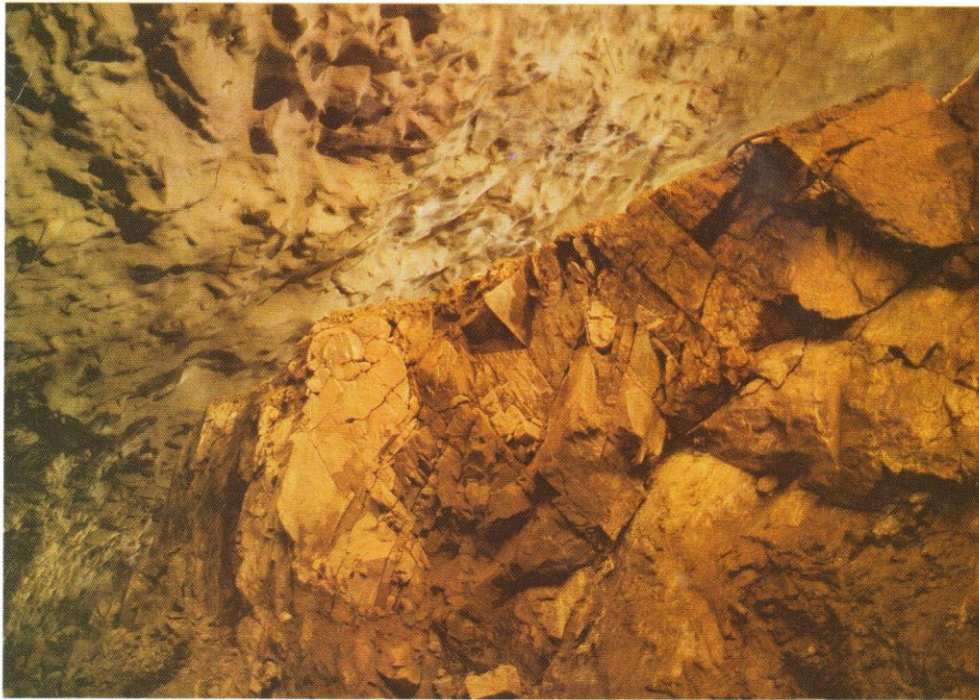


Fig. 27. Photograph of typical jointing viewed parallel to cavern axis. Note marked overbreak beneath 10 cm of S(fr).

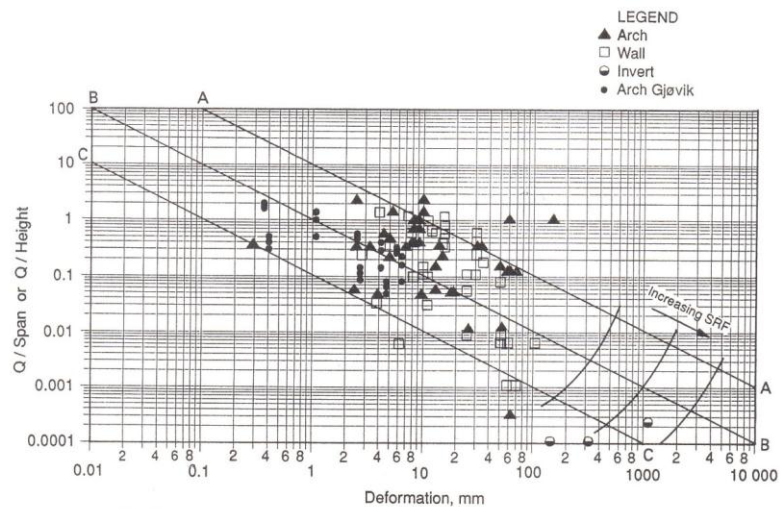


Fig. 28. Olympic cavern arch displacements compared to *Q*-system database.

Acknowledgements—The authors would like to thank members of the User Group who have provided generous support of the research project: Veidekke and Selmer (whose JV was responsible for cavern construction), Dyno Industries, Fortifikasjon, NOTEBY, SINTEF, NGI, Østlandsforskning, the Municipality of Gjøvik, Statoil, Statkraft, Televerket, BeFo (Sweden) and Hyundai (South Korea).

Accepted for publication 23 April 1994.

REFERENCES

1. Brown E. T. and Hoek E. Trends in relationships between measured *in situ* stresses and depth. *Int. J. Rock Mech. Min. Sci. & Geomech. Abstr.* **15**, 211–215 (1978).
2. Barton N. and Hansteen H. Very large span openings at shallow depth: deformation magnitudes from jointed models and F.E. analysis. *Proceedings of the 4th Rapid Excavation and Tunnelling Conference*, Atlanta, GA, Chap. 77, pp. 1331–1353 (1979).
3. Grimstad E., Barton N., Lien R., Lunde J. and Løset F. Classification of rock masses with respect to tunnel stability—new experiences with the *Q*-system. In *Fjellsprenningsteknikk, Bergmekanikk, Geoteknikk*. Tapir Press, Oslo (1986) (in Norwegian).
4. Grimstad E. and Barton N. Updating of the *Q*-system for NMT. *Proceedings of the International Symposium on Sprayed Concrete*, Fargenes, Norway (Edited by Kompen, Opsahl and Berg). Norwegian Concrete Association, Oslo (1993).
5. Cundall P. A. A generalized distinct element program for modelling jointed rock. Report PCAR-1-80, Contract DAJA37-79-C-0548, European Research Office, US Army. Peter Cundall Associates (1980).
6. Makurat A., Barton N., Vik G., Chryssanthakis P. and Monsen K. Jointed rock mass modelling. *Proceedings of the International Symposium on Rock Joints*, Loen, Norway, pp. 647–656 (1990).
7. By T.L. Geotomography for rock mass characterisation and prediction of seepage problems for two main road tunnels under the City of Oslo. *Proceedings of the International Congress on Rock Mechanics (ISRM)*, Montreal, Canada, pp. 37–40 (1987).
8. Barton N., Grimstad E., Aas G., Opsahl O. A., Bakken A., Pedersen L. and Johansen E. D. Norwegian Method of Tunnelling, WT focus. *World Tunnelling* June and August (1992).
9. Barton N. Application of *Q*-system and index tests to estimate shear strength and deformability of rock masses. *Proceedings of the International Symposium on Engineering Geology and Underground Construction*, Lisbon, Portugal, Vol. 2, pp. II.51–II.70 (1983).
10. Bieniawski Z. T. Rock mass classification in rock engineering. *Proceedings of the Symposium on Exploration for Rock Engineering*, Johannesburg, South Africa, Vol. 1, pp. 97–106 (1976).
11. Barton N. and Bandis S. C. Review of predictive capabilities of JRC–JCS model in engineering practice. *Proceedings of the International Symposium on Rock Joints*, Loen, Norway, pp. 603–610 (1990).
12. Løset F. and Bhasin R. Engineering geology—Gjøvik Ice Hockey Cavern. Research Project: “Publikumshall i Berg”. SINTEF/NGI/Østlandsforskning, Norway (1992).
13. Morseth B. and Løset F. Rock cavern stadium—pre-investigations—decision base—excavation. Final Report on the Research Project for the Rock Cavern Stadium. NGI/SINTEF/Østlandsforskning, Norway (1993).
14. Kristiansen J. and Hansen S. E. Rock Cavern Stadium—displacement measurements. Final Report on the Research Project for the Rock Cavern Stadium. NGI/SINTEF/Østlandsforskning, Norway (1993).
15. Barton N., Løset F., Lien R. and Lunde J. Application of the *Q*-system in design decisions concerning dimensions and appropriate support for underground installations. *Proceedings of the International Conference on Sub-surface Space*, Rockstore, Stockholm, Vol. 2, pp. 553–561 (1980).